On the Interplay between Charge-Shift Bonding and Halogen Bonding

Serigne Sarr, Jérôme Graton, Gilles F Montavon, Julien Pilmé, Nicolas Galland

FULL PAPER

On the Interplay Between Charge-Shift Bonding and Halogen Bonding

Serigne Sarr,[a] Jérôme Graton,[a] Gilles Montavon,[b] Julien Pilmé,*[c] and Nicolas Galland*[a]

Abstract: The nature of halogen-bond interactions has been analysed from the perspective of the astatine element, which is potentially the strongest halogen-bond donor. Relativistic quantum calculations on complexes formed between halide anions and a series of $Y_3C–X$ (Y = F to X, X = I, At) halogen-bond donors disclosed unexpected trends, *e.g.*, $At_3C–At$ revealing a weaker donating ability than $I_3C–I$ despite a stronger polarizability. All the observed peculiarities have their origin in a specific component of C–Y bonds: the charge-shift bonding. Descriptors of the Quantum Chemical Topology show that the halogen-bond strength can be quantitatively anticipated from the magnitude of charge-shift bonding operating in $Y_3C–X$. The charge-shift mechanism weakens the ability of the halogen atom X to engage in halogen bonds. This outcome provides rationales for outlier halogen-bond complexes, which are at variance with the consensus that the halogen-bond strength scales with the polarizability of the halogen atom.

1. Introduction

The anisotropy of the electron density distribution in a covalently bonded halogen atom (X) can induce a site of attractive interactions with a nucleophilic region from another, or from the same, molecular entity. Halogen bond (XB) interactions are prevalent in many areas of chemistry,[1–7] demonstrating important applications in catalysis,[8–11] crystal engineering[12–14] and rational drug design.[15–18] From a fundamental point of view, it has as well become a topic of main interest in the computational chemistry community.[19–21] Politzer and co-workers showed that the halogen lone-pairs, perpendicular to the covalent R-X bond, form a belt of negative electrostatic potential, leaving on the extension of the R-X bond an area of positive electrostatic potential.[22] This electrophilic cap depicts the so-called "σ-hole". Many correlations were established between the maximum value of the molecular electrostatic potential, $V_{s,max}$, calculated at the σ-hole and the stabilisation energies of the corresponding XBs.[19,23–26] Beyond the electrostatically-driven component, Politzer and co-workers invoked the need to consider a contribution of polarisation to describe some particular XBs, forging this way the concept of Coulombic σ-hole.[19,27] Some authors opposed other contributions, including dispersion, charge transfer (leading to partial covalent bond formation), and the repulsive component resulting from the Pauli exclusion principle.[28–37]

The controversy remains strong, as can be noted from the recent literature on the emblematic case of the $Y_3C–I$ halogen-bond donor.[38–41] While studying the XB interactions between $Y_3C–I$ (Y = F to I) and the Cl^- and NMe_3 Lewis bases, Huber and co-workers highlighted unexpected trends regarding the interaction strengths.[38] Going down along the halogen column, the Y substituent becomes more polarisable but less electronegative, it exerts a weaker electron-withdrawing power at the iodine atom, lowering the electrophilic character at the σ-hole of this latter. The $V_{s,max}(I)$ descriptor became indeed smoothly less positive, but the XB strength conversely increased in the order Y = F < Cl < Br < I. The authors concluded for a contradiction to "the general consensus that more electronegative (carbon-based) groups R, bound to the electrophilic halogen atom X, will lead to more stable complexes of R–X with Lewis bases." In their subsequent investigations based on different schemes of energy decomposition analysis,[39,40] Huber and co-workers argued that the charge transfer, acting against the Pauli repulsion, drives the evolution of the interaction energies in $Y_3C–I\cdots Z^-$ (Y = F to I, Z = F to Br) systems. This conclusion was soon challenged, from a physical perspective, by Clark *et al*.[41] They extended the study to Z = F to I, and demonstrated that the Coulombic σ-hole concept completely explains the formation of $Y_3C–I\cdots Z^-$ complexes. Using a distant unit point charge (PC) to approximate the polarising effect of the halide anion Z^-, the computed most positive electrostatic potential at the iodine's σ-hole, $V_{s,max}(PC)$, was found to nicely correlate with XB interaction energies.

A natural extension of these recent works is to consider the case where the XB-donor atom, iodine, is substituted by astatine (At). Indeed, astatine is to date the heaviest halogen element and the most polarisable one.[42] It is therefore appealing to probe the XB interaction in $Y_3C–X\cdots Z^-$ systems from the perspective of the most potent XB-donor element. Astatine (Z = 85) is a radioelement whose second long-lived isotope, At-211, has been recently identified as being of high potential interest for nuclear medicine applications.[43] Some of us reported recently the very first experimental investigation of XBs mediated by astatine.[44] Since no conventional spectroscopic tools can be used, the conclusions were notably supported by quantum mechanical calculations. Astatine being a heavy element, relativistic treatments must be used and include *a priori* both spin-

[a] *S. Sarr, Dr. J. Graton, Dr. N. Galland*
CEISAM, UMR CNRS 6230
Université de Nantes, F-44000 Nantes (France)
E-mail: nicolas.galland@univ-nantes.fr
[b] *Dr. G. Montavon*
SUBATECH, UMR CNRS 6457
IMT Atlantique, F-44307 Nantes (France)
[c] *Dr. J. Pilmé*
Laboratoire de Chimie Théorique, UMR CNRS 7616
Sorbonne Université, F-75005 Paris (France)
E-mail: pilme@lct.jussieu.fr

Supporting information and the ORCID identification number(s) for the author(s) of this article can be found under:

independent (scalar) and spin-dependent effects. The relativistic effects can be sizeable on the ability of astatine to form XBs, modifying by several tens of percent the interaction energies.[26,45] Scalar-relativistic (sr) effects are associated with the mass-increase of core electrons resulting essentially from their high speed. The main spin-dependent effect, arising from the interaction of the electron spin with magnetic fields generated by other charged particles in relative motion, is the spin-orbit coupling (SOC). We have recently shown that the influence of SOC can be used as a powerful tool to probe the mechanism of XB interactions.[46] By "turning on" or "off" this relativistic effect in the quantum calculations, we disclosed a connection between the astatine propensity to form charge-shift bonds and the strength of the XBs in $AtX\cdots NH_3$ (X = F to At) complexes. Following this strategy, we propose in this work to investigate the nature of the interaction in $Y_3C–X\cdots Z^-$ (Y = F to At, Z = Cl, I, At) systems with X = At, and some with X = I for comparison purpose.

2. Results and Discussion

2.1. When astatine does not follow trends

Scalar-relativistic results and benchmarking. As mentioned above, the $Y_3C–I\cdots Z^-$ systems with Y and Z = F to I have been thoroughly studied in the literature,[38–41] and our objective is to extend these investigations to the astatine systems. However, it is worth noticing that the reported interaction energies for the $Y_3C–I\cdots Z^-$ systems show large disparities. For instance, the interaction energy in the case of $I_3C–I\cdots Cl^-$ ranges from -183.7 kJ/mol at the PBE/TZ2P level of theory,[38] to -131.4 kJ/mol at the MP2/aug-cc-pVTZ level of theory.[41] Thus, it seems necessary to establish first quality benchmark data for such systems (see the Computational section for the description of the methodology and acronyms).

The geometries of the $Y_3C–X\cdots Z^-$ systems with Y = F to At, X = I, At, and Z = Cl, I, At have therefore been optimized at the counterpoise corrected (CP) sr-CCSD/AVTZ level of theory, providing accurate XB interaction distances ($d_{X\cdots Z}$ values gathered in Table S1 in Supporting Information, SI). These geometries were used to compute interaction energies using the "gold standard" CCSD(T) method at the complete basis set limit (see ΔE^{CP} values in Table S1). These data can be used to check the accuracy of the selected DFT functionals and atomic basis sets for this work. Our B3LYP/AVTZ and PW6B95/AVTZ results obtained at the same relativistic level are presented in Table S1. The sr-B3LYP/AVTZ calculations yield results in excellent agreement, with a mean signed error (MSE) of -1.0 kJ/mol and a mean absolute error (MAE) of 2.3 kJ/mol (2.0%) with respect to the computed sr-CCSD(T)/CBS interaction energies. The interaction distances are slightly shorter than the CP sr-CCSD/AVTZ calculated ones, with the MSE and MAE values of -0.037 Å and 0.037 Å (1.2%), respectively. Very close results are obtained at the sr-PW6B95/AVTZ level of theory, but with slightly higher MSE and MAE values (for example, the MAE values are 2.8% and 2.3% for the interaction energies and distances, respectively). Hence, the two selected levels of theory are well suited to study the $Y_3C–X\cdots Z^-$ systems with Y = F – At, X = I, At, and Z = Cl, I, At. Solely the B3LYP/AVTZ results will be commented hereinafter, but identical trends are observed with the PW6B95 DFT functional.

All the studied $Y_3C–X\cdots Z^-$ systems exhibit a C_{3v} symmetry, *i.e.*, the C, X and Z atoms are perfectly aligned, and the corresponding $d_{X\cdots Z}$ distances are, at least, shorter than the sum of the van der Waals radii for neutral X and Z atoms.[47] These geometrical characteristics are attributes of XB complexes. The evolutions of the interaction strengths (ΔE^{CP}) as a function of the halogen substituent Y are presented in Figure 1. We note that, for given Lewis base Z^- and substituent Y, the interaction in $Y_3C–X\cdots Z^-$ systems is stronger when the XB is mediated by astatine than by iodine. This result corroborates the calculated greater lengthening of the C–X bond upon complexation when the At atom is the XB donor ($\Delta d_{C–X}$ values in Table S1). Indeed, we can anticipate a weakening of the C–X bond when the XB is strengthened, leading to a greater lengthening of the corresponding distance. For instance, the interaction energy and C–X bond lengthening for the $F_3C–At\cdots Cl^-$ system are -119.3 kJ/mol and +0.080 Å, while those for $F_3C–I\cdots Cl^-$ are -99.4 kJ/mol and +0.063 Å. Huber and co-workers,[38,40] as well as Clark *et al.*,[41] have previously shown that the interaction strength of the I-mediated XB increases monotonously from Y = F to I in the $Y_3C–I\cdots Z^-$ (Y, Z = F, Cl, Br and I) systems. Our calculated interaction energies are in line with this trend for iodine (Figure 1), but an original behaviour is observed with astatine in the $Y_3C–At\cdots Z^-$ systems. Even if the interaction is still strengthened from Y = F to I, it is unexpectedly weakened when Y = At. For instance, the interaction energy in the $Y_3C–At\cdots Cl^-$ systems ranges from -119.3 kJ/mol (Y = F) to -149.8 kJ/mol (Y = I) and then decreases to -145.3 kJ/mol (Y = At). This surprising behaviour is even confirmed with the iodide (Figure 1) and astatide anions as acceptors. The evolution of the interaction energy is supported by those of the $X\cdots Z^-$ interaction distance and of the C–X bond lengthening (Table S1). For example, the $d_{X\cdots Z}$ distance is monotonously shortened in $Y_3C–At\cdots Cl^-$ systems from 2.853 Å to 2.736 Å when Y = F to I, and is finally lengthened to 2.742 Å with Y = At.

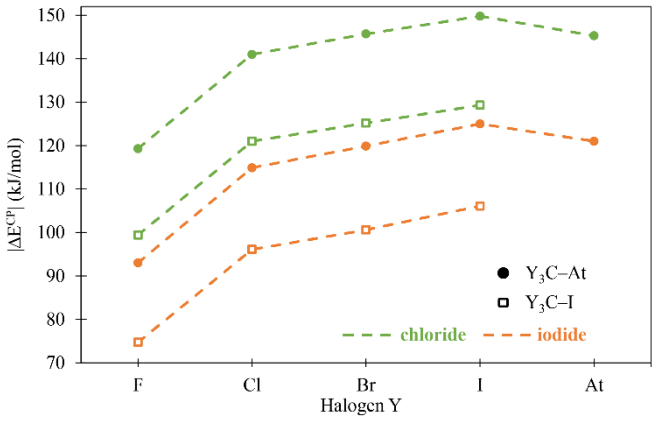

Figure 1. Evolution of the halogen-bond interaction energy computed for $Y_3C–X\cdots Z^-$ systems (Z = Cl, I), at the sr-B3LYP/AVTZ level of theory.

Table 1. 2c-B3LYP/AVTZ counterpoise-corrected interaction energy of the $Y_3C–I\cdots Z^-$ systems (kJ/mol).

	Cl^-		I^-		At^-	
	ΔE^{CP}	ΔSO[a]	ΔE^{CP}	ΔSO[a]	ΔE^{CP}	ΔSO[a]
$F_3C–At$	-122.2	-2.9	-94.0	-1.0	-91.7	-0.9
$Cl_3C–At$	-142.9	-1.9	-113.9	1.0	-113.9	-0.1
$Br_3C–At$	-147.9	-2.2	-118.7	1.1	-119.8	-0.7
$I_3C–At$	-150.2	-0.4	-121.4	3.6	-124.3	0.6
$At_3C–At$	-130.2	15.1	-102.2	18.8	-105.3	15.8
$F_3C–I$	-99.8	-0.4	-74.8	-0.1	–	–
$Cl_3C–I$	-121.4	-0.4	-96.2	-0.1	–	–
$Br_3C–I$	-125.3	-0.1	-100.4	0.2	–	–
$I_3C–I$	-126.9	2.4	-102.6	3.5	-112.4	-5.8

[a] The spin-orbit effect (ΔSO) is defined as the difference between the results of 2c- and sr-B3LYP/AVTZ calculations.

Two-component relativistic results. When they involve heavy elements such as astatine, the systems discussed above are affected by relativistic effects, which have been taken into account through scalar-relativistic (sr) calculations. Nevertheless, many studies have demonstrated that the quantum calculations should also include the relativistic spin-orbit interaction for At-containing compounds.[42,44,48–53] For instance, the interaction energy of At-mediated XBs can be affected by SOC effects up to 35%.[26,45,46] Hence, all these systems have been additionally investigated through two-component (2c) relativistic calculations. The energetic results are gathered in Table 1, and the corresponding structural data are reported in SI, Table S3. The spin-orbit coupling effect (ΔSO) is estimated through the difference between 2c-B3LYP/AVTZ and sr-B3LYP/AVTZ results.

In the iodine series, *i.e.*, the $Y_3C–I\cdots Z^-$ systems, SOC effects are almost negligible on the interaction energies and geometric parameters. Nevertheless, the SOC is found for $I_3C–I$ to markedly affect the halogen-bond interaction: ΔE^{CP} becomes more negative by 1.9% and 3.2% for Z = Cl and I, respectively, and less negative by 5.4% for Z = At. For a given $Y_3C–I$ monomer, a systematic and significant weakening of the interaction energies is found from Cl^- to I^- as Lewis base. Conversely, a strengthening can be observed with At^-: the interaction energies obtained for $I_3C–I\cdots At^-$ and $I_3C–I\cdots I^-$ are -112.4 and -102.6 kJ/mol, respectively.

Focusing on the astatine series, *i.e.*, the $Y_3C–At\cdots Z^-$ systems, a systematic lengthening of the XB interaction distances appears upon SOC effects (Table S3). For a given Lewis base, the lengthening increases from Y = F to At. This regular trend is actually not reproduced on the energy scale, since SOC effects can lead to either an increase or a decrease of the interaction energies. In the case of $At_3C–At$ as XB donor, there is a systematic and strong lessening of the interaction energies, at least by 15.1 kJ/mol with chloride Lewis base and on average by 13% (whatever the Z^- anion under study). As displayed in SI on Figure S1, the SOC effects are so important that $At_3C–At$, which was a similar XB donor than $Br_3C–At$ at the scalar-relativistic level, becomes competed by $F_3C–At$ at the 2c-relativistic level of theory. This finding supports the scalar-relativistic results discussed above: while the XB interaction strength increases from Y = F to I, it drops with Y = At (Table 1). Hence, the strengthening of the interaction when Y goes down along the halogen column, previously shown by Clark *et al.* and Huber and co-workers for the $Y_3C–I\cdots Z^-$ systems,[38,40,41] is not generalizable.

Table 2. Average interaction distances and dissociation energies for some $Y_3C–X\cdots Z^-$ systems, and bond lengths and dissociation energies for XZ molecules, obtained from 2c-B3LYP calculations with a triple zeta basis set.

	$Y_3C–X\cdots Z^-$		X–Z	
	$< d_{X\cdots Z} >$	$< D_e >$[a]	$d_{X–Z}$	D_e
X = I, Z = Cl	2.75	118	2.36[b]	192[b]
X = I, Z = I	3.15	94	2.73[c]	122[c]
X = At, Z = Cl	2.86	139	2.52[c]	–
X = At, Z = I	3.20	110	2.88[c]	–
X = At, Z = At	3.33	111	3.05[c]	63[c]

[a] $D_e = |\Delta E^{CP}|$ for the $Y_3C–X\cdots Z^-$ systems. [b] Values from Ref. [54]. [c] Values from Refs. [55,56].

Astatinated compounds question another well-established trend in the field of halogen bonding. In general, the polarizability increase of the halogen element, acting as XB donor, leads to an increase of the XB strength.[7] Despite astatine is known to have a higher polarizability than iodine,[42] $At_3C–At$ exhibits in some cases weaker XB energies than its lighter homologue $I_3C–I$. Indeed, if the stabilization of the $At_3C–At\cdots Cl^-$ complex is higher than the $I_3C–I\cdots Cl^-$ structure by 3.3 kJ/mol, the interaction energies with iodide are similar for $At_3C–At$ and $I_3C–I$, and most importantly the $At_3C–At\cdots At^-$ system is a weaker XB complex than $I_3C–I\cdots At^-$ by 7.1 kJ/mol (Table 1). This inversion between the ability of $At_3C–At$ and $I_3C–I$ to engage in XB interactions when the halide anion is changed, from Cl^- to I^- and finally to At^-, is also confirmed by the 2c-PW6B95/AVTZ results gathered in SI, Table S4. This behaviour, only disclosed with SOC, strongly points out the requirement to include in quantum mechanics calculations the spin-dependent relativistic effects for an accurate description of At-containing systems.

An additional point questioned by our 2c-relativistic results is related to the nature itself of the XB interaction in the $Y_3C–X\cdots Z^-$ (Y = F to At, X = I, At and Z = Cl, I, At) systems. Indeed, it appears at first that the $d_{X\cdots Z}$ interaction distances and the bond lengths reported for the X–Z dihalogen molecules,[54–56] as well as their respective dissociation energies, are unexpectedly not so different. These data, gathered in Table 2, show for instance that the average $d_{At\cdots At}$ distance in $Y_3C–At\cdots At^-$ systems is only 9% longer than the bond length calculated in diastatine (at the same level of theory), the $d_{I\cdots I}$ distance in $Y_3C–I\cdots I^-$ systems being also only 16% longer than the bond length in diiodine. In addition, their dissociation energies are of the same order of magnitude: $D_e(Y_3C–I\cdots I^-)$ is about 76% of $D_e(I_2)$. The average dissociation

energy for the $Y_3C–At\cdots At^-$ systems is even significantly larger than the dissociation energy of At_2, at the same level of theory. These outcomes are evidences of non-classical XBs, which cannot be regarded as non-bonding, non-covalent, or weak interactions.

2.2. Relationship with charge-shift bonding

Assessment of the $V_{s,max}$(PC) descriptor. Since the seminal study of Huber *et al.*,[38] it is well established that the $V_{s,max}$ value at the iodine's σ-hole is not suitable to explain the evolution of the interaction energies in $Y_3C–I\cdots Z^-$ series. This finding is confirmed for the astatinated homologues. Indeed, the $V_{s,max}$ value at the astatine's σ-hole in $Y_3C–At$ donors decreases from Y = F to At (Table S5 in SI), despite the enhancement of the XB strength at least from Y = F to I (*cf.* ΔE^{CP} values in Table 1). To date, the $V_{s,max}$(PC) descriptor recently introduced by Clark *et al.* represents the best explicative parameter of the XB magnitude in $Y_3C–I\cdots Z^-$ systems.[41] $V_{s,max}$(PC) is the perturbed value of $V_{s,max}$, calculated for the ground-state XB donor, in presence of a unit negative point charge (PC) at the location of Z in the complex. Clark *et al.* found a very good correlation with the interaction energies in $Y_3C–I\cdots Z^-$ systems with Z = F to I. The coefficient of determination r^2 is of 0.994 for a data set of 16 points, even if these authors noticed that the interaction energies computed for the iodide Lewis base slightly deviate from the correlation, showing a somewhat family dependency.

This analysis has been extended to the case of $Y_3C–At$ donors, with Z = Cl, I and At, representing a set of 15 couples of $V_{s,max}$(PC) and ΔE^{CP} values computed at the 2c-B3LYP/AVTZ level of theory. These data exhibit a true correlation, with an associated coefficient of determination r^2 of 0.859 (Figure S2 in SI), but significantly deteriorated with respect to that obtained by Clark *et al*. for a data set dominated by light-halide Lewis bases. It is obvious from Figure 2 that family-dependent relationships appear when the different Lewis bases (Cl^-, I^- and At^-) are distinguished. Improved individual correlations between the interaction energy and $V_{s,max}$(PC) have been found for the $Y_3C–At$ donors interacting with chloride (r^2 = 0.889), iodide (r^2 = 0.973) and astatide (r^2 = 0.913). Hence, $V_{s,max}$(PC) still appears as a pertinent descriptor of the XB strength in $Y_3C–X\cdots Z^-$ systems, provided that X and Z are fixed.

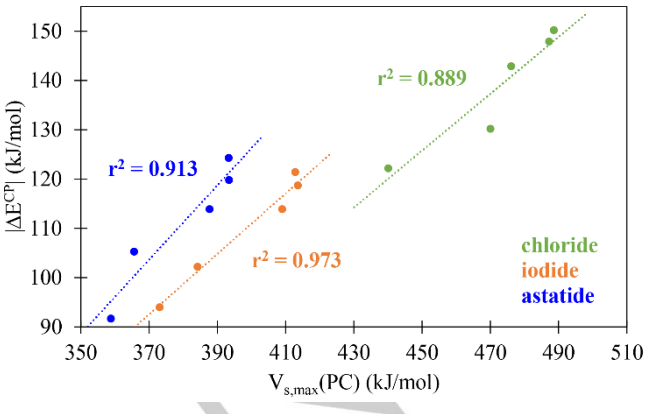

Figure 2. Relationships between the interaction energies in $Y_3C–At\cdots Z^-$ and the $V_{s,max}$(PC) values computed for astatine in $Y_3C–At$ at the 2c-B3LYP/AVTZ level of theory. The coefficient of determination is shown for each Z^- Lewis base.

According to Clark *et al.*,[41] the $V_{s,max}$(PC) represents the maximum value of the polarised molecular electrostatic potential at the X σ-hole in the $Y_3C–X$ monomer, the polarisation being due to the negative point charge that mimics the halide anion. Hence, in their interpretation of the Coulombic σ-hole, $V_{s,max}$(PC) accounts for the electrostatics with polarisation approximately included, and this provides a satisfactory, physically-based explanation of the interaction in $Y_3C–X\cdots Z^-$ systems. Note nevertheless that the polarizability being a tensor property, the point charge cannot obviously account for the complete polarisation due to the electric field generated by the halide anion. Furthermore, a deeper analysis of our data suggests that other mechanisms may contribute to the stability of these systems. Indeed, focusing at the $Y_3C–At$ donors and replacing Y = I by more polarisable At atoms, we would anticipate an increase of the $Y_3C–At$ polarizability, and of its XB-donating ability according to Clark *et al.* conjecture.[41] Nevertheless, $I_3C–At$ leads systematically to stronger interactions than $At_3C–At$ (*cf.* ΔE^{CP} values in Table 1). In the same vein, $At_3C–At$ would be a more potent XB donor than $I_3C–I$ according to Clark *et al*. This assumption is at odds with our results. It was also demonstrated elsewhere that At_2 is a weaker XB donor than I_2.[26,46] The good correlation between the interaction energies and computed $V_{s,max}$(PC) values leads us to consider that $V_{s,max}$(PC) encompasses additional physics to the simulated polarisation due to the halide Lewis base.

Insight from the perturbed electron density. Indices of a specific component were obtained by analysing the changes, upon introduction of the point charge at the Z^- position, on the electron density of unperturbed $Y_3C–X$. Such analysis was performed as well by Clark *et al*.,[41] but our attention is hereafter focused at the characteristics of the XB-donor atom (X). Figure 3 shows the electron density modifications for $I_3C–At$ and $At_3C–At$ when the unit negative charge was placed at the position of the chloride anion in the $Y_3C–At\cdots Cl^-$ complexes. Obviously, a large loss of electron density is induced in the region of astatine's σ lone-pair, which is close and points to the unit negative charge. The resulting electronic redistribution, at short-distance, is mainly

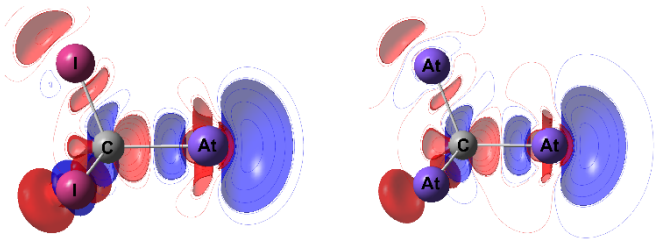

Figure 3. Modifications of the 2c-B3LYP/AVTZ calculated electron density for $I_3C–At$ (left) and $At_3C–At$ (right) upon introduction of a unit negative charge at the position of the chloride anion in the respective complexes. The surfaces (isovalue = 0.0011 a.u.) in red colour show the areas with a significant increase of electron density and in blue colour the areas with a significant decrease. A spacing of 0.0001 a.u. is used for the contour plots.

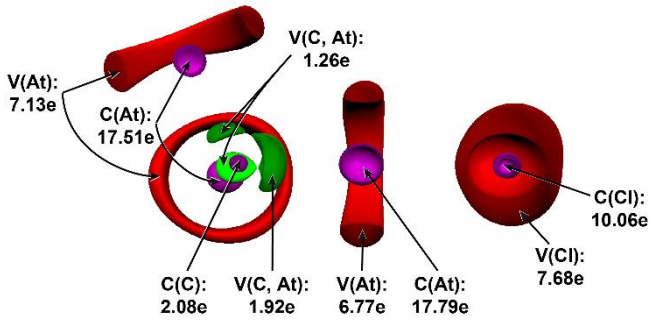

Figure 4. Cross-section of ELF localisation domains for the $At_3C–At\cdots Cl^-$ complex (isosurface = 0.786, the At atom in front of the plane was removed) and respective electron populations at the 2c-B3LYP/AVTZ level of theory. Colour code: magenta for core basins, red for valence non-bonding basins and green for bonding basins.

towards a physical space that surrounds the astatine atom as a ring perpendicular to the C–At bond (represented in its entirety for $I_3C–At$ on Figure S3 in SI). It can be identified to the classical belt of negative electrostatic potential, associated to the π lone-pairs of the XB donor. This mechanism of electronic redistribution, from the σ to the π system representing the lone-pairs of the XB-donor atom, is also illustrated for $F_3C–At$ and $I_3C–I$ on Figure S4 in SI. Moreover, such mechanism is fully in line with the lone-pair bond-weakening effect (LPBWE), which was first discussed in the 80s by R. T. Sanderson.[57] The LPBWE is associated to three-electron repulsions between the bonding electrons and the lone-pairs, adjacent to the bond, which have the same symmetry as the bond (here σ). This repulsive interaction weakens the spin-pairing bonding, hence bond stabilisation is achieved by moving the electron-pair density away from the σ system.[58] The unit negative charge can be viewed here as approximately simulating a bonding electron, provided by the Lewis base to the XB interaction, which interacts with the σ lone-pair, leading to LPBWE and a distinct contribution to the calculation of $V_{s,max}$(PC).

The LPBWE does not preclude the formation of bonds and can be offset by adjusting the electron-pair density, giving rise to charge-shift (CS) bonding.[58] CS bonds form a class of bonds that emerged recently alongside the two traditional covalent and ionic bond families.[59,60] CS bonding consists in a large and dynamic fluctuations of the bonding electron-pair, resulting in an important resonance energy between the covalent and ionic structures ($^-$A| B^+ ↔ A–B ↔ $^+$A |B^-). Electronegative and/or lone-pair-rich elements such as halogens are prone to form CS bonds, and it appears from the previous discussion that $V_{s,max}$(PC) accounts for the ability of the XB-donor atom to bind through CS bonding.

Topological analyses of the XB complexes. Further indices of a CS-bonding component to the XB interaction in $Y_3C–X\cdots Z^-$ systems are provided by the Quantum Chemical Topology. It gathers different methods that use rigorous mathematical formalisms to establish bridges between the modern quantum mechanical wave functions and the traditional chemical concepts. In general, these methods divide the 3D physical space into electronic volumes or basins endowed with chemical meaning. For example, the topological analysis of the Electron Localisation Function (ELF) associates the electron density to core basins around nuclei A, labelled C(A), and valence basins.[61] These can be either non-bonding basins, corresponding to lone-pairs of a A atom and labelled V(A), or bonding basins, characterizing the covalent character of bonds between two A atoms and labelled V(A_1, A_2).

Figure 4 displays the ELF localisation domains determined for $At_3C–At\cdots Cl^-$ and the electron populations of the ELF basins. Note that the core-basin populations are close to 18 core electrons for the At atoms (60 core electrons being implicitly treated *via* a pseudo-potential), to 10 core electrons for the Cl atom, and to 2 core electrons for the C atom. The V(At, C) bonding basins reveal populations below the characteristic value of two electrons, corresponding to the case of the ideal covalent bond in Lewis theory. Connections between CS bonding and halogen bonding in $At_3C–At\cdots Cl^-$ become clear (i) when focusing at the lone-pairs of the XB-donor atom, described by the non-bonding V(At) basin, and (ii) by using as a tool the SOC to probe the XB interaction. At the 2c-B3LYP/AVTZ level of theory, the V(At) population exceeds the three lone-pairs expected in Lewis theory for a monovalent halogen atom. The total electron population is of 6.77, with a π contribution of 3.71 electrons (*i.e.*, the electron density described by *p* orbitals perpendicular to the C–At bond). Interestingly, the comparison with the results from sr-calculations indicates that the π population of V(At) is increased with SOC by 0.50 electron at the expense of the σ one. It appears a strong similarity between this SOC-induced electron redistribution in the complex and the electron redistribution previously described when a unit negative charge is placed away from the XB donor. Hence, SOC balances the LPBWE by adjusting σ and π densities in the lone-pair region, which is a manifestation of CS bonding. This outcome is consistent with previous results indicating that

Table 3. Selected QTAIM descriptors (in a.u.) obtained at the 2c-B3LYP/AVTZ level of theory for the XB interaction in $Y_3C–At\cdots Cl^-$ systems.

	integrated		at the BCP of the XB interaction		
	q(Cl)[b]	δ(At, Cl)[c]	ρ_b[d]	$\nabla^2\rho_b$[e]	$\lvert V_b\rvert/G_b$[f]
Y = F	-0.77	0.56	0.039	0.075	1.20
ΔSO[a]	-0.01	-0.02	-0.005	0.001	-0.02
Y = Cl	-0.72	0.62	0.045	0.080	1.25
ΔSO[a]	-0.01	-0.03	-0.003	0.001	-0.03
Y = Br	-0.71	0.64	0.047	0.081	1.27
ΔSO[a]	-0.01	-0.05	-0.002	0.001	-0.03
Y = I	-0.69	0.65	0.047	0.082	1.27
ΔSO[a]	-0.03	-0.06	-0.002	0.001	-0.04
Y = At	-0.74	0.61	0.044	0.080	1.25
ΔSO[a]	-0.07	-0.09	-0.005	0.001	-0.05

[a] The spin-orbit effect is defined as the difference between the results of 2c- and sr-B3LYP/AVTZ calculations. [b] Atomic charge. [c] Delocalisation index. [d] Electron density. [e] Laplacian of the electron density. [f] Ratio between the potential energy density and the (positive definite) kinetic energy density.

SOC enhances the ability of astatine to form CS bonds.[46,56,62]

The contribution of CS bonding to XB interactions in Y_3C–At···Cl^- is also witnessed by different descriptors of the Quantum Theory of Atoms In Molecules (QTAIM). QTAIM is the theoretical framework for studying the topology of the total electron density, ρ(r), and provides a route to analyse, evaluate and classify the nature of chemical bonds and interactions.[63] QTAIM basins are atomic and topological atoms can be defined as the union of a nucleus and of its atomic basin. Table 3 reports the computed charge of the chloride anion, from which it is easy to estimate a significant charge transfer from the halide anion to Y_3C–At, ranging between 0.23 and 0.31 electrons. In the context of halogen bonding, charge transfer is associated to a covalent component. Because (i) the SOC enhances the propensity of astatine to form CS bonds,[46,56] and (ii) the CS mechanism tends to weaken covalency (*via* large and dynamic ionic-covalent mixing),[58–60] the SOC lowers by 8% on average the charge transfer (*cf.* negative ΔSO values for q(Cl) in Table 3).

In the same vein, we scrutinized the SOC effect on a QTAIM descriptor computed at the bond critical point (BCP, the point of minimum electron density on the bond path) of the XBs. The ratio between the potential (V) and positive definite kinetic (G) energy densities at the BCP, $|V_b|/G_b$, reflects the covalency magnitude within the interaction.[63,64] Note that G_b is obtained here from a fictitious Kohn-Sham system of non-interacting electrons. The results presented in Table 3 show that all XB interactions in Y_3C–At···Cl^- systems satisfy $|V_b|/G_b > 1$, indicating a covalent component (the potential energy density dominates and electrons are stabilized at the BCP). SOC systematically lessens the $|V_b|/G_b$ ratio (*cf.* negative ΔSO values), *i.e.*, the covalency, due to the increased CS character.

The most impressive characteristic is the high value of the delocalisation index between At and Cl atoms, δ(At, Cl) ranging from 0.56 to 0.65 (Table 3). Considered as a measure of the sharing of electron-pairs between atoms,[63,65] δ is found in the literature to have a value approaching to zero for the so-called non-bonding or weak interactions, meanwhile it shows values approaching to the formal bond order for covalent and CS bonds.[66] For instance, these δ values significantly differ from those obtained from crystal structures of exceptionally short O···F XBs, between 0.02 and 0.05,[67] and those corresponding to characteristic XB interactions in complexes between diiodine and substituted pyridines, between 0.27 and 0.41;[68] all these values being obtained at an analogous level of theory (B3LYP/6-311G**). Consequently, such δ(At, Cl) values in Y_3C–At···Cl^- systems indicate an important degree of exchanged electrons between At and Cl atoms, associated to a covalent and/or CS component. Note that the same trends can also be drawn from the QTAIM descriptors either obtained from PW6B95/AVTZ calculations (Table S6 in SI) or calculated on the Y_3C–I···Cl^- systems (Table S7 in SI).

2.3. Rationales from the XB donor's properties

Electron density distribution at the XB-donor atom. The $V_{s,max}$(PC) descriptor, introduced by Clark *et al.*,[41] have demonstrated a two folded interest. It accurately reproduces the evolution of the interaction energy in Y_3C–X···Z^- systems, provided that X and Z are fixed, and, it provides a route to disclose the main components, including CS bonding, of the corresponding XB interactions. However, it is not possible to anticipate the interaction strength without having previously studied the XB complex: the computation of $V_{s,max}$(PC) requires to formerly determine the structure of the complex (*i.e.*, its stability). We have investigated the possibility that, from the quantum chemical topology analysis of the Y_3C–X donors, some descriptors (i) can be appropriate to predict the interaction strength in the corresponding complexes with halide anions, and, at the same time (ii) bring some insight on the nature of the formed XBs. In the coming analysis, the following considerations will be relevant:

- In the H_3C–Y species, the C–Y bond was previously described in the literature as a CS bond if Y = F or At,[56,59] while for Y = Cl, the C–Cl bond is depicted as a borderline case between the traditional polar covalent bond and the charge-shift bond.[69]
- The weakest XB donor in the Y_3C–I series presents three C–F bonds, and the following one three C–Cl bonds. The analogy is more striking regarding the Y_3C–At donors, since the weakest ones exhibit C–Y bonds with Y = F and At, and then follows Y = Cl (*cf.* ΔE^{CP} values in Table 1).

Since the $V_{s,max}$(PC) descriptor has led to family-dependent relationships, we focused first on establishing, for a given series

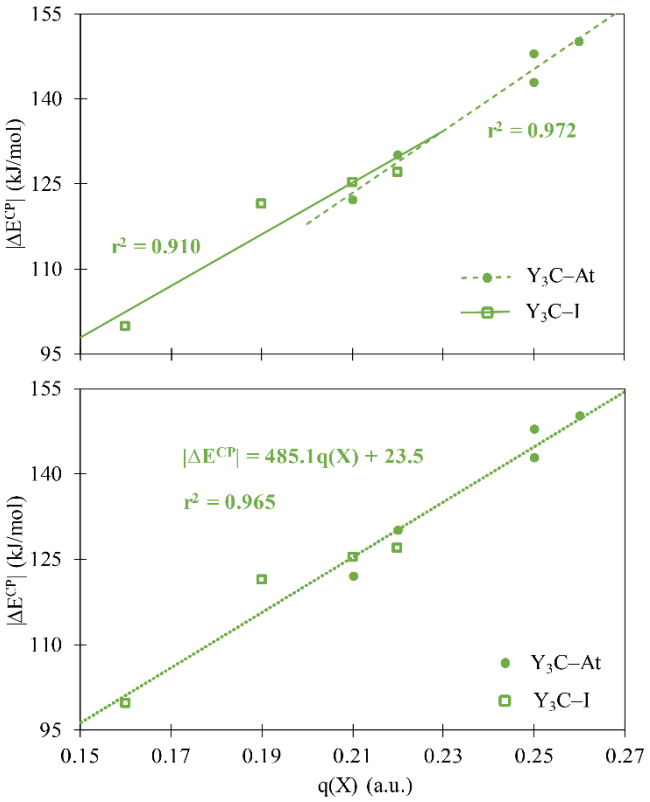

Figure 5. Correlations between the interaction energy in Y_3C–X···Cl^- and the QTAIM charge computed for X in isolated XB donors at the 2c-B3LYP/AVTZ level of theory. Top: distinct relationships corresponding either to X = I or X = At; bottom: merged data for X = I and X = At.

Table 4. Selected QTAIM descriptors (in u.a.) obtained at the 2c-B3LYP/AVTZ level of theory for the $Y_3C–X$ donors.

	q(C)[a]	q(Y)[a]	q(X)[a]	C–Y bonds				C–X bond			
				δ[b]	ρ_b[c]	$\nabla^2\rho_b$[d]	$\lvert V_b\rvert/G_b$[e]	δ[b]	ρ_b[c]	$\nabla^2\rho_b$[d]	$\lvert V_b\rvert/G_b$[e]
$F_3C–At$	1.74	-0.65	0.21	0.68	0.289	-0.303	2.21	0.84	0.098	0.027	1.85
$Cl_3C–At$	0.17	-0.14	0.25	1.09	0.192	-0.243	2.90	0.84	0.087	0.037	1.76
$Br_3C–At$	-0.25	0.00	0.25	1.10	0.149	-0.104	2.48	0.87	0.087	0.042	1.74
$I_3C–At$	-0.88	0.21	0.26	1.08	0.111	-0.016	2.09	0.91	0.086	0.044	1.72
$At_3C–At$	-0.90	0.22	0.22	0.98	0.088	0.044	1.72	0.98	0.088	0.044	1.72
$F_3C–I$	1.79	-0.65	0.16	0.68	0.293	-0.346	2.24	0.93	0.120	-0.041	2.21
$Cl_3C–I$	0.17	-0.12	0.19	1.08	0.193	-0.242	2.90	0.98	0.111	-0.023	2.13
$Br_3C–I$	-0.24	0.01	0.21	1.09	0.149	-0.104	2.48	1.02	0.112	-0.019	2.11
$I_3C–I$	-0.87	0.22	0.22	1.08	0.111	-0.016	2.09	1.08	0.111	-0.016	2.09

[a] Atomic charge. [b] Delocalisation index. [c] Electron density. [d] Laplacian of the electron density. [e] Ratio between the potential energy density and the (positive definite) kinetic energy density.

of XB donors (X = I or X = At), distinct relationships corresponding to the different halides (Z = Cl, I and At). It was done separately at the two relativistic levels (sr and 2c), leading for instance to a total of six distinct relationships for the astatine series. Based on the QTAIM analysis of the $Y_3C–X$ electron densities, we attempted to correlate atomic charges with the interaction energies in $Y_3C–X\cdots Z^-$ systems. The computed atomic charges at the 2c-B3LYP/AVTZ level of theory are gathered in Table 4, while examples of correlation are displayed on Figure 5.

Striking good correlations were obtained when considering the q(X) charge. From the six distinct relationships associated to the astatine series (three possible Z^- halides, two different relativistic levels), the average coefficient of determination is 0.957 (individual r^2 values are gathered in Table S10 of SI). In addition, the corresponding average coefficient of determination for the iodine series is 0.934. It is noticeable that the q(X) value in a given series (X = I or X = At) does not evolve according to the electron-withdrawing power of the Y atoms. While the q(Y) charge decreases with the increased electronegativity of Y, and the q(C) charge increases accordingly, q(X) decreases for instance in $Y_3C–I$ from +0.22 electrons when Y = I to +0.16 electrons when Y = F. In fact, q(Y) and q(C) exhibit weak correlations with the XB interaction energy. The outstanding correlation between the q(X) charge and the interaction energy is definitely not related to Y's electron-withdrawing power.

It is worth noting that the QTAIM charges take into account the anisotropy of the electron distribution in the atomic basins, these latter being obviously not spherical. Furthermore, strong relationships exist between the full set of q(X) charges computed for the $Y_3C–X$ (X = I and At) donors and the strength of the XB interactions with a given halide anion. As shown on Figure 5, the interaction energies in $Y_3C–X\cdots Cl^-$ complexes correlate with q(X) charges computed on the isolated donors with $r^2 = 0.965$. The corresponding coefficient of determination for the XB complexes with iodide anion is 0.950 (Figure S5 in SI.).

Influence of vicinal CS bonds. Having unveiled a genuine descriptor of the XB-donor atom that enables anticipating the interaction strength in the $Y_3C–X\cdots Z^-$ systems, we continue our investigations to identify the factors affecting q(X) when Y is changed in the $Y_3C–X$ donors. q(Y) being put aside, we investigate some ELF descriptors related to Y and in particular the valence bonding basins of C–Y bonds. As earlier mentioned, a bonding basin in ELF topology characterizes the bond covalent character. A deviation of its electron population from the two electrons expected for the ideal single covalent bond in Lewis theory, would indirectly points out other contributions, *e.g.*, ionic and/or CS bonding.

In the astatine series (X = At), Table 5 reports for V(C, Y) electron populations of 1.12 and 1.47 for Y = F and At, respectively. This most likely indicates, in addition to covalency, a significant ionic or/and CS contribution. Note that the electron fluctuation from these V(C, F) and V(C, At) basins through the whole molecule, quantified by the variance σ^2 (Table 5), is particularly large. It represents 70% and 65% of the electron population of these basins, respectively. In the framework of ELF topological analyses, the population and its variance for bonding-basins are considered to provide a measure of electron delocalisation (for compounds with highly delocalised π systems such as benzene, the relative variance for the bonding basins is about 50% or less).[70] It is also stated that a large variance in addition to a depleted basin population is the signature of a significant CS bonding character,[58,60] since "covalent-ionic mixing is associated with fluctuation of the electron-pair from the average electron population".[71]

It is remarkable that the weakest XB donors exhibit the most depleted V(C, Y) basins. In fact, it exists a true correlation between the electron population of V(C, Y) and the XB interaction energies. From the six distinct relationships associated to the astatine series (three possible Z^- halides, two different relativistic levels), the average coefficient of determination is 0.894 (*cf*. Table

Table 5. ELF electron population analysis of $Y_3C–X$ donors obtained at the 2c-B3LYP/AVTZ level of theory.

	C(X)[a]	V(X)[a]	V(C, X)		V(C, Y)	
			pop[a]	σ^{2}[b]	pop[a]	σ^{2}[b]
$F_3C–At$	17.50	6.95	1.76	1.04	1.12	0.78
$Cl_3C–At$	17.50	6.95	1.68	1.00	1.52	0.96
$Br_3C–At$	17.50	6.95	1.67	1.00	1.53	0.97
$I_3C–At$	17.50	6.95	1.58	0.98	1.60	1.00
$At_3C–At$	17.50	6.96	1.47	0.95	1.47	0.95
$F_3C–I$	17.72	6.66	1.79	1.02	1.13	0.79
$Cl_3C–I$	17.72	6.65	1.70	1.01	1.53	0.96
$Br_3C–I$	17.72	6.63	1.70	1.01	1.56	0.97
$I_3C–I$	17.72	6.61	1.61	1.00	1.61	1.00

[a] Electron population in a.u. [b] Variance of the electron population in a.u.

S10 for individual r^2 values). The hypothesis that the gradual deviation of these basin populations to two electrons is due to an increasing CS character is supported by the similar value of the average coefficient of determination, 0.885, obtained when correlating the variance of these basins with the six sets of interaction energies. The evolution of the interaction strength in $Y_3C–At\cdots Z^-$ complexes appears therefore related to the CS contribution in C–Y bonds.

Since the CS mechanism is non-local in nature ("resonance fluctuation" of the electron-pair between physical-space domains attached to the bonded atoms), one should consider its possible extension to the vicinal C–X bond. Indeed, the C–X bonds exhibit significant fluctuations of the electron population associated to their ELF bonding basins, as witnessed by the σ^2 values reported in Table 5 (about one electron). Furthermore, we have obtained a significantly improved, average coefficient of determination of 0.914 from the six possible linear regressions, in the astatine series, between the summed variances of all bonding basins and the XB interaction energies in $Y_3C–At\cdots Z^-$ complexes (*cf.* Table S10 for individual r^2 values). This outcome is strengthened when considering the corresponding average coefficient of determination obtained for the iodine series (X = I): 0.995. Hence, the CS mechanism acting in C–Y bonds seems to spread through the C–X bond, affecting the electron density distribution at the X atom so as to rule its ability to engage in XBs. In summary, the disclosed relationships provide a qualitative and quantitative understanding of the factor, *i.e.*, the magnitude of the CS bonding acting in the whole XB donor, that drives the evolution of the interaction strength in $Y_3C–X\cdots Z^-$ systems. As final illustration, the situations where $At_3C–At$ appears as a weaker XB donor than $I_3C–I$ only occur at the 2c-relativistic level of theory, *i.e.*, when SOC is accounted for, and SOC effects are known to enhance the propensity of astatine to form CS bonds.[46,56] It is a striking manifestation of the interplay between CS bonding and halogen bonding.

3. Conclusions

The ability of $Y_3C–X$ (Y = F to X, X = I and At) species to form halogen-bond (XB) interactions with halide anions has been thoroughly investigated. Two-component relativistic quantum mechanical calculations have confirmed for the iodine series (X = I) that the evolution of the interaction energy is contradictory with the general consensus that XBs are strengthened as the substituent group bound to X halogen atom is more electron-withdrawing. Furthermore, within the astatine series (X = At), after a monotonous increase of the XB interaction energies from Y = F to I, a strong drop is observed for Y = At ($At_3C–At$ being a weaker XB donor than $I_3C–At$, $Br_3C–At$ and even $Cl_3C–At$). In addition, $At_3C–At$ also appears to have a weaker ability to form XB interactions than $I_3C–I$. These findings strongly disagree with the assumption, widely shared in the community, that a more polarisable halogen atom would yield stronger XBs. All these peculiarities have been rationalised from the contribution of charge-shift (CS) bonding. The CS mechanism consists in large and dynamic fluctuations of the bonding electron density. CS bonds are typified by an important resonance energy between the covalent and ionic Lewis structures ($^-A|\ B^+ \leftrightarrow A–B \leftrightarrow {}^+A\ |B^-$).[60]

On the basis of mathematically well-defined descriptors, either derived from a physical perspective (electrostatic potential and polarizability) or from traditional chemical concepts (quantum chemical topology analyses), we have uncovered a CS bonding component to the interaction in $Y_3C–X\cdots Z^-$ (Z = Cl, I, At) complexes. In addition, the CS character of C–Y bonds in the XB donor appears as the main explicative factor for the variation of the interaction energies when the Y atom is varied. The CS mechanism spreads through the C–X bond and affects the electron density distribution at the X atom. Determined from the Quantum Theory of Atoms In Molecules, the X atomic charge embeds information on the anisotropy of the electron distribution into electrostatics. Then, simple calculations of $Y_3C–X$ intrinsic properties, such as q(X), allow us to quantitatively anticipate the stability of potential XB complexes, as illustrated by the correlation shown in Figure 5. *In fine*, the disclosed elements indicate as a whole that the magnitude of CS bonding operating in the $Y_3C–X$ donor weakens its ability to engage in XB interactions. The same reasoning was previously held to rationalise the weaker donating ability of At_2 with respect to I_2,[46] and it most probably applies to the very recently reported XBs formed by multivalent astatine in AtY_3 and AtY_5 (Y = F to I) donors: the interaction energy increases from Y = F to Cl and then monotonously decreases.[72]

4. Computational Section

4.1. Quantum chemical calculations

The two-component relativistic density functional theory, which was proved to be accurate for investigation of At-containing systems,[73,74,49,50,75,55] requires to replace the orbital representation by spinors that are complex vector functions of two components (2c). Both the Generalized Kohn-Sham (GKS) method, implemented in the Gaussian program,[76] and the Spin-Orbit DFT (SODFT) method, implemented in the NWChem program,[77] take advantages of relativistic pseudo-potentials

containing scalar and spin-dependent terms to treat the electron correlation and relativistic effects on an equal footing.

There can be many variations in the form of relativistic pseudo-potentials, those used in this work are expressed as follows:[78]

$$\hat{\mathrm{V}}(r) = -\frac{\mathrm{Z_{eff}}}{r} + \sum_{klj} \mathrm{B}_{lj}^{k} \exp\left(-\beta_{lj}^{k}\, r^{2}\right) \hat{\mathrm{P}}_{lj} \qquad (1)$$

where Z_{eff} is the charge of the inner-core. The sum runs over a gaussian expansion (index *k*) of semi-local short-range radial potentials, which are different for different orbital angular-momentum quantum numbers *l*, and, for a given *l*, for the two total one-electron angular-momentum quantum numbers $j = l \pm ½$. $\hat{\mathrm{P}}_{lj}$ is the 2c projector onto the complete space of functions with angular symmetry *l*, *j* around the core under study. The parameters B_{lj}^{k} and β_{lj}^{k} are adjusted so that $\hat{\mathrm{V}}$ in 2c valence-only atomic calculations reproduces, as closely as possible, a set of relativistic all-electron multiconfiguration Dirac-Hartree-Fock (MCDHF) energies. Note that a transcription of such kind of pseudo-potentials into a scalar-relativistic spin-averaged part (averaged relativistic potential $\hat{\mathrm{V}}_{\mathrm{AREP}}$) and an effective one-electron spin-orbit operator ($\hat{\mathrm{V}}_{\mathrm{SO}}$) is easily possible.[79]

Gaussian 16 rev. A.03 was used to perform the geometry optimisations and frequency calculations with the global hybrid B3LYP and PW6B95 functionals.[80,81] They have been recommended in a recent benchmark study focused on At-species,[53] and have been furthermore validated as reliable for investigating compounds stabilised by At-mediated halogen bonds.[26,44,46] The small-core pseudo-potentials ECP*n*MDF with *n* = 60, 28 and 10 were used for the At, I and Br atoms, respectively.[78,82] Their remaining electrons were described using the triple-zeta aug-cc-pVTZ-PP basis sets,[78,82] supplemented for the At and I atoms by 2c extensions.[83] The aug-cc-pVTZ basis sets were used for the C, F and Cl atoms,[84–86] and the whole set of basis functions is abbreviated as AVTZ. The energy of the $Y_3C–X\cdots Z^-$ systems were corrected from the basis set superposition error (BSSE) using the counterpoise method.[87] In order to assess the SOC effects, geometry optimizations and frequency calculations were also carried out at the scalar-relativistic level of theory, *i.e.*, in absence of spin-dependent terms in the pseudo-potentials ($\hat{\mathrm{V}}_{\mathrm{AREP}}$ only).

In order to assess the reliability of the B3LYP/AVTZ and PW6B95/AVTZ calculations, some *ab initio* coupled cluster calculations were performed, at the scalar-relativistic level of theory for species involving heavy atoms. The frozen-core approximation was used in all those calculations, *e.g.*, the 5s5p5d electrons of At were kept frozen as well as the 1s electrons of C atom. Geometry optimizations were performed at the CCSD/AVTZ level of theory, using counterpoise (CP) corrections in the case of $Y_3C–X\cdots Z^-$ systems. Then, single point CCSD(T) calculations[88] were performed on top of the previously optimized CP-CCSD/AVTZ geometries, using the AVTZ basis sets, the corresponding double-zeta variant (referred to as AVDZ) and the quadruple-zeta variant (referred to as AVQZ). For each species, an estimates of the CCSD(T) energy at the complete basis set limit (CBS) was produced by combining:

- the Hartree-Fock energy obtained from the three-point extrapolation formulae of Feller:[89]

$$E_X = E_{\mathrm{CBS}} + Be^{-\alpha X} \qquad (2)$$

where *X* is the cardinal number of the basis sets, *i.e.*, 2 for AVDZ, 3 for AVTZ and 4 for AVQZ. The E_{CBS} energy, α and B parameters are then determined from three computed Hartree-Fock energies.

- the correlation energy obtained from the two-point extrapolation scheme USTE(*x*-1,*x*) of Varandas and co-workers:[90]

$$E_X^{\mathrm{corr}} = E_{\mathrm{CBS}}^{\mathrm{corr}} + \frac{A}{x^3} \qquad (3)$$

where *x* is simply referred as hierarchical number. In case of coupled cluster calculations, *x* = 2.71 when *X* = 3 and *x* = 3.68 when *X* = 4. The two correlation energies from CCSD(T) calculations using AVTZ and AVQZ basis sets, allowed us to determine both the A parameter and the $E_{\mathrm{CBS}}^{\mathrm{corr}}$ correlation energy.
The interaction energies at CBS are then calculated following the super-molecule approach.

Introduced by Becke and Edgecombe,[91] the Electron Localization Function (ELF) is a signature of the distribution of electronic pairs and the analysis of its topology is a powerful tool for the characterization of bonding schemes.[61] Furthermore, it is found from experimental and theoretical reports that the Quantum Theory of Atoms In Molecules (QTAIM), defined by Bader, can be used to gain insight into the nature of the chemical bonding.[63,92] QTAIM atomic charges were calculated by subtracting the electron population of the topological atom to its atomic number (eventually decreased by the pseudo-potential charge). Details on the extension of the ELF and QTAIM topological analysis in the framework of 2c-DFT calculations can be found in Refs. [55] and [56]. All the topological analyses were carried out using modified versions of NWChem 5.1.1 and the TopChem2 standalone program.[93] The relevant program files, which implement the treatment of 2c-wavefunctions, are freely available upon request.

4.2. Theoretical developments

Introduced by Bader and Stephens,[94] and revivified later by Fradera *et al.*,[95] the QTAIM concept of delocalization index, noted $\delta(\Omega_{\mathrm{A}}, \Omega_{\mathrm{B}})$, is connected to the number of electron-pairs shared between two basins, Ω_{A} and Ω_{B}, and can be compared to other bond order indices. At the DFT level of theory, second-order densities based on the single determinant of Kohn–Sham orbitals are used even though they are an approximation to the unknown exact DFT second-order density.[96] For closed-shell systems, the first-order matrix can be expanded in terms of molecular orbitals φ_i. Then, the δ is expressed as:

$$\delta(\Omega_{\mathrm{A}}, \Omega_{\mathrm{B}}) = 2 \sum_{i} \sum_{j} < \varphi_i | \varphi_j >_{\Omega_{\mathrm{A}}} < \varphi_i | \varphi_j >_{\Omega_{\mathrm{B}}} \qquad (4)$$

where $< \varphi_i | \varphi_j >_{\Omega_{\mathrm{A}}}$ and $< \varphi_i | \varphi_j >_{\Omega_{\mathrm{B}}}$ are the overlaps between molecular orbitals, integrated respectively within the atomic basins Ω_{A} and Ω_{B}. The summation in the equation (4) runs over all the occupied molecular spin-orbitals of the molecule.

The nonrelativistic single determinant formalism operating with orbitals can be extended to a 2c-relativistic formalism where the wave function is built from normalized single-particle functions known as (pseudo-)spinors, $\varphi_i(r)$. The latter are no longer of pure spin character, but have both one α and one β complex component, and hence, two components:

$$\varphi_i(r) = \begin{pmatrix} \varphi_{i\alpha}(r) \\ \varphi_{i\beta}(r) \end{pmatrix} \qquad (5)$$

For closed-shell systems, the partial overlap between orbitals involved in the equation (4) can be easily extended to the 2c-spinors:

$$\begin{aligned} < \varphi_i | \varphi_j >_{\Omega_{\mathrm{A}}} &= \int_{\Omega_{\mathrm{A}}} \varphi_i^{\dagger}(r) \varphi_j(r)\, \mathrm{d}r \\ &= \int_{\Omega_{\mathrm{A}}} \left(\varphi_{i\alpha}^{*}(r) \varphi_{j\alpha}(r) + \varphi_{i\beta}^{*}(r) \varphi_{j\beta}(r) \right) \mathrm{d}r \\ &= < \varphi_{i\alpha} | \varphi_{j\alpha} >_{\Omega_{\mathrm{A}}} + < \varphi_{i\beta} | \varphi_{j\beta} >_{\Omega_{\mathrm{A}}} \end{aligned} \qquad (6)$$

Therefore,

$$\delta(\Omega_A,\Omega_B) = 2\sum_i\sum_j[(<\varphi_{i\alpha}|\varphi_{j\alpha}>_{\Omega_A} + <\varphi_{i\beta}|\varphi_{j\beta}>_{\Omega_A})(<\varphi_{i\alpha}|\varphi_{j\alpha}>_{\Omega_B} + <\varphi_{i\beta}|\varphi_{j\beta}>_{\Omega_B})] \quad (7)$$

This formulation can readily be calculated from occupied 2c-spinors and is safe for practical use on closed-shell species where the spin polarisation is small (Kramers-restricted closed-shell approximation).

In the framework of the ELF topological analysis, the integration of the electron density over the volume of a Ω basin provides its population, $\bar{N}(\Omega)$. The variance, noted $\sigma^2[\Omega]$, is a signature of the fluctuating density (delocalisation) from a given basin through the whole molecule.[70] It represents the quantum mechanical uncertainty on $\bar{N}(\Omega)$. In the two-component formalism, σ^2 can be calculated from occupied 2c-spinors as follows:

$$\sigma^2[\Omega] = \bar{N}(\Omega) - \sum_i\sum_j |<\varphi_{i\alpha}|\varphi_{j\alpha}>_{\Omega} + <\varphi_{i\beta}|\varphi_{j\beta}>_{\Omega}|^2 \quad (8)$$

Acknowledgements

This work has been supported in part by grants from the French National Agency for Research called “Programme d’Investissements d’Avenir” (ANR-11-EQPX-0004, ANR-11-LABX-0018, ANR-16-IDEX-0007) and from the “Région Pays de la Loire”. It was carried out using HPC resources from CCIPL (“Centre de Calcul Intensif des Pays de la Loire”).

Keywords: astatine • relativistic effects • quantum chemical topology • noncovalent interactions • bond theory

[1] H. L. Nguyen, P. N. Horton, M. B. Hursthouse, A. C. Legon, D. W. Bruce, *J. Am. Chem. Soc.* **2004**, *126*, 16–17.
[2] P. Metrangolo, F. Meyer, T. Pilati, G. Resnati, G. Terraneo, *Angew. Chem., Int. Ed.* **2008**, *47*, 6114–6127.
[3] R. Wilcken, M. O. Zimmermann, A. Lange, A. C. Joerger, F. M. Boeckler, *J. Med. Chem.* **2013**, *56*, 1363–1388.
[4] G. Berger, J. Soubhye, F. Meyer, *Polym. Chem.* **2015**, *6*, 3559–3580.
[5] E. Persch, O. Dumele, F. Diederich, *Angew. Chem., Int. Ed.* **2015**, *54*, 3290–3327.
[6] B. Li, S.-Q. Zang, L.-Y. Wang, T. C. W. Mak, *Coord. Chem. Rev.* **2016**, *308*, 1–21.
[7] G. Cavallo, P. Metrangolo, R. Milani, T. Pilati, A. Priimagi, G. Resnati, G. Terraneo, *Chem. Rev.* **2016**, *116*, 2478–2601.
[8] S. M. Walter, F. Kniep, E. Herdtweck, S. M. Huber, *Angew. Chem., Int. Ed.* **2011**, *50*, 7187–7191.
[9] D. Bulfield, S. M. Huber, *Chem. Eur. J.* **2016**, *22*, 14434–14450.
[10] M. Breugst, D. von der Heiden, J. Schmauck, *Synthesis* **2017**, *49*, 3224–3236.
[11] L. Carreras, M. Serrano-Torné, P. W. N. M. van Leeuwen, A. Vidal-Ferran, *Chem. Sci.* **2018**, *9*, 3644–3648.
[12] A. Farina, S. V. Meille, M. T. Messina, P. Metrangolo, G. Resnati, G. Vecchio, *Angew. Chem., Int. Ed.* **1999**, *38*, 2433–2436.
[13] F. Meyer, P. Dubois, *CrystEngComm* **2013**, *15*, 3058–3071.
[14] A. Mukherjee, S. Tothadi, G. R. Desiraju, *Acc. Chem. Res.* **2014**, *47*, 2514–2524.
[15] A. R. Voth, F. A. Hays, P. S. Ho, *PNAS* **2007**, *104*, 6188–6193.
[16] Y. Lu, Y. Liu, Z. Xu, H. Li, H. Liu, W. Zhu, *Expert Opin. Drug Discov.* **2012**, *7*, 375–383.
[17] Z. Xu, Z. Yang, Y. Liu, Y. Lu, K. Chen, W. Zhu, *J. Chem. Inf. Model.* **2014**, *54*, 69–78.
[18] C. Ren, X. Ding, A. Roy, J. Shen, S. Zhou, F. Chen, S. F. Y. Li, H. Ren, Y. Y. Yang, H. Zeng, *Chem. Sci.* **2018**, *9*, 4044–4051.
[19] P. Politzer, J. S. Murray, T. Clark, *Phys. Chem. Chem. Phys.* **2013**, *15*, 11178–11189.
[20] L. P. Wolters, P. Schyman, M. J. Pavan, W. L. Jorgensen, F. M. Bickelhaupt, S. Kozuch, *Wiley Interdiscip. Rev. Comput. Mol. Sci.* **2014**, *4*, 523–540.
[21] M. H. Kolář, P. Hobza, *Chem. Rev.* **2016**, *116*, 5155–5187.
[22] T. Clark, M. Hennemann, J. S. Murray, P. Politzer, *J. Mol. Model.* **2007**, *13*, 291–296.
[23] K. E. Riley, J. S. Murray, P. Politzer, M. C. Concha, P. Hobza, *J. Chem. Theory Comput.* **2009**, *5*, 155–163.
[24] K. E. Riley, J. S. Murray, J. Fanfrlík, J. Řezáč, R. J. Solá, M. C. Concha, F. M. Ramos, P. Politzer, *J. Mol. Model.* **2011**, *17*, 3309–3318.
[25] M. Kolář, J. Hostaš, P. Hobza, *Phys. Chem. Chem. Phys.* **2014**, *16*, 9987–9996.
[26] N. Galland, G. Montavon, J.-Y. Le Questel, J. Graton, *New J. Chem.* **2018**, *42*, 10510–10517.
[27] P. Politzer, J. S. Murray, T. Clark, *J. Mol. Model.* **2015**, *21*, 52.
[28] K. E. Riley, P. Hobza, *J. Chem. Theory Comput.* **2008**, *4*, 232–242.
[29] J. G. Hill, X. Hu, *Chem. Eur. J.* **2013**, *19*, 3620–3628.
[30] C. Wang, D. Danovich, Y. Mo, S. Shaik, *J. Chem. Theory Comput.* **2014**, *10*, 3726–3737.
[31] J. Řezáč, A. de la Lande, *Phys. Chem. Chem. Phys.* **2016**, *19*, 791–803.
[32] L. P. Wolters, F. M. Bickelhaupt, *ChemistryOpen* **2012**, *1*, 96–105.
[33] K. E. Riley, P. Hobza, *Phys. Chem. Chem. Phys.* **2013**, *15*, 17742–17751.
[34] C. Wang, L. Guan, D. Danovich, S. Shaik, Y. Mo, *J. Comput. Chem.* **2016**, *37*, 34–45.
[35] M. D. Santis, F. Nunzi, D. Cesario, L. Belpassi, F. Tarantelli, D. Cappelletti, F. Pirani, *New J. Chem.* **2018**, *42*, 10603–10614.
[36] B. Zheng, Y. Liu, L. Huang, Z. Wang, H. Liu, Y. Liu, *Mol. Phys.* **2018**, *116*, 1834–1843.
[37] L. N. Anderson, F. W. Aquino, A. E. Raeber, X. Chen, B. M. Wong, *J. Chem. Theory Comput.* **2018**, *14*, 180–190.
[38] S. M. Huber, E. Jimenez-Izal, J. M. Ugalde, I. Infante, *Chem. Commun.* **2012**, *48*, 7708–7710.
[39] S. M. Huber, J. D. Scanlon, E. Jimenez-Izal, J. M. Ugalde, I. Infante, *Phys. Chem. Chem. Phys.* **2013**, *15*, 10350–10357.
[40] J. Thirman, E. Engelage, S. M. Huber, M. Head-Gordon, *Phys. Chem. Chem. Phys.* **2018**, *20*, 905–915.
[41] T. Clark, A. Heßelmann, *Phys. Chem. Chem. Phys.* **2018**, *20*, 22849–22855.
[42] T. Fleig, A. J. Sadlej, *Phys. Rev. A* **2002**, *65*, 032506.
[43] G. Vaidyanathan, M. R. Zalutsky, *Curr. Radiopharm.* **2008**, *1*, 177–196.
[44] N. Guo, R. Maurice, D. Teze, J. Graton, J. Champion, G. Montavon, N. Galland, *Nat. Chem.* **2018**, *10*, 428–434.
[45] P. Matczak, *Mol. Phys.* **2018**, *116*, 338–350.
[46] J. Graton, S. Rahali, J.-Y. L. Questel, G. Montavon, J. Pilmé, N. Galland, *Phys. Chem. Chem. Phys.* **2018**, *20*, 29616–29624.
[47] M. Mantina, A. C. Chamberlin, R. Valero, C. J. Cramer, D. G. Truhlar, *J. Phys. Chem. A* **2009**, *113*, 5806–5812.
[48] T. Saue, K. Faegri, O. Gropen, *Chem. Phys. Lett.* **1996**, *263*, 360–366.
[49] D. Peng, W. Liu, Y. Xiao, L. Cheng, *J. Chem. Phys.* **2007**, *127*, 104106.
[50] J. Champion, M. Seydou, A. Sabatié-Gogova, E. Renault, G. Montavon, N. Galland, *Phys. Chem. Chem. Phys.* **2011**, *13*, 14984–14992.
[51] A. Severo Pereira Gomes, F. Réal, N. Galland, C. Angeli, R. Cimiraglia, V. Vallet, *Phys. Chem. Chem. Phys.* **2014**, *16*, 9238–9248.
[52] R. Maurice, F. Réal, A. Severo Pereira Gomes, V. Vallet, G. Montavon, N. Galland, *J. Chem. Phys.* **2015**, *142*, 094305.
[53] D.-C. Sergentu, G. David, G. Montavon, R. Maurice, N. Galland, *J. Comput. Chem.* **2016**, *37*, 1345–1354.
[54] W. K. Cho, Y. J. Choi, Y. S. Lee, *Mol. Phys.* **2005**, *103*, 2117–2122.

[55] J. Pilmé, E. Renault, T. Ayed, G. Montavon, N. Galland, *J. Chem. Theory Comput.* **2012**, *8*, 2985–2990.
[56] J. Pilmé, E. Renault, F. Bassal, M. Amaouch, G. Montavon, N. Galland, *J. Chem. Theory Comput.* **2014**, *10*, 4830–4841.
[57] R. T. Sanderson, *Polar Covalence*, Academic Press, **1983**.
[58] S. Shaik, D. Danovich, B. Braida, W. Wu, P. C. Hiberty, in *The Chemical Bond II*, Springer, Cham, **2015**, pp. 169–211.
[59] S. Shaik, P. Maitre, G. Sini, P. C. Hiberty, *J. Am. Chem. Soc.* **1992**, *114*, 7861–7866.
[60] S. Shaik, D. Danovich, W. Wu, P. C. Hiberty, *Nat. Chem.* **2009**, *1*, 443–449.
[61] B. Silvi, A. Savin, *Nature* **1994**, *371*, 683–686.
[62] M. Amaouch, G. Montavon, N. Galland, J. Pilmé, *Mol. Phys.* **2016**, *114*, 1326–1333.
[63] C. F. Matta, R. J. Boyd, *The Quantum Theory of Atoms in Molecules: From Solid State to DNA and Drug Design*, Wiley-VCH, Weinheim, **2007**.
[64] D. Cremer, E. Kraka, *Angew. Chem., Int. Ed.* **1984**, *23*, 627–628.
[65] C. Outeiral, M. A. Vincent, Á. M. Pendás, P. L. A. Popelier, *Chem. Sci.* **2018**, *9*, 5517–5529.
[66] B. Silvi, R. J. Gillespie, C. Gatti, in *Comprehensive Inorganic Chemistry II (Second Edition)* (Eds.: J. Reedijk, K. Poeppelmeier), Elsevier, Amsterdam, **2013**, pp. 187–226.
[67] A. Sirohiwal, V. R. Hathwar, D. Dey, R. Regunathan, D. Chopra, *Acta Cryst. B* **2017**, *73*, 140–152.
[68] E. V. Bartashevich, E. A. Troitskaya, V. G. Tsirelson, *Chem. Phys. Lett.* **2014**, *601*, 144–148.
[69] A. Shurki, P. C. Hiberty, S. Shaik, *J. Am. Chem. Soc.* **1999**, *121*, 822–834.
[70] A. Savin, B. Silvi, F. Colonna, *Can. J. Chem.* **1996**, *74*, 1088–1096.
[71] S. Shaik, D. Danovich, B. Silvi, D. L. Lauvergnat, P. C. Hiberty, *Chem. Eur. J.* **2005**, *11*, 6358–6371.
[72] F. Zhou, Y. Liu, Z. Wang, T. Lu, Q. Yang, Y. Liu, B. Zheng, *Phys. Chem. Chem. Phys.* **2019**, *21*, 15310–15318.
[73] Y. J. Choi, Y. S. Lee, *J. Chem. Phys.* **2003**, *119*, 2014–2019.
[74] A. V. Mitin, C. van Wüllen, *J. Chem. Phys.* **2006**, *124*, 064305.
[75] D.-D. Yang, F. Wang, *Phys. Chem. Chem. Phys.* **2012**, *14*, 15816–15825.
[76] M. J. Frisch, G. W. Trucks, H. B. Schlegel, G. E. Scuseria, M. A. Robb, J. R. Cheeseman, G. Scalmani, V. Barone, G. A. Petersson, H. Nakatsuji, et al., *Gaussian 16 Rev. A.03*, Wallingford, CT, **2016**.
[77] T. P. Straatsma, E. Apra, T. L. Windus, E. J. Bylaska, W. A. de Jong, S. Hirata, M. Valiev, M. Hackler, L. Pollack, R. J. Harrison, *NWChem, A Computational Chemistry Package for Parallel Computers*, Pacific Northwest National Laboratory: Richland, Washington, **2008**.
[78] K. A. Peterson, D. Figgen, E. Goll, H. Stoll, M. Dolg, *J. Chem. Phys.* **2003**, *119*, 11113–11123.
[79] M. Dolg, X. Cao, *Chem. Rev.* **2012**, *112*, 403–480.
[80] P. J. Stephens, F. J. Devlin, C. F. Chabalowski, M. J. Frisch, *J. Phys. Chem.* **1994**, *98*, 11623–11627.
[81] Y. Zhao, D. G. Truhlar, *J. Phys. Chem. A* **2005**, *109*, 5656–5667.
[82] K. A. Peterson, B. C. Shepler, D. Figgen, H. Stoll, *J. Phys. Chem. A* **2006**, *110*, 13877–13883.
[83] M. K. Armbruster, W. Klopper, F. Weigend, *Phys. Chem. Chem. Phys.* **2006**, *8*, 4862–4865.
[84] T. H. Dunning, *J. Chem. Phys.* **1989**, *90*, 1007–1023.
[85] R. A. Kendall, T. H. Dunning, R. J. Harrison, *J. Chem. Phys.* **1992**, *96*, 6796–6806.
[86] D. E. Woon, T. H. Dunning, *J. Chem. Phys.* **1993**, *98*, 1358–1371.
[87] S. F. Boys, F. Bernardi, *Mol. Phys.* **1970**, *19*, 553–566.
[88] G. D. Purvis, R. J. Bartlett, *J. Chem. Phys.* **1982**, *76*, 1910–1918.
[89] D. Feller, *J. Chem. Phys.* **1992**, *96*, 6104–6114.
[90] F. N. N. Pansini, A. C. Neto, A. J. C. Varandas, *Chemical Physics Letters* **2015**, *641*, 90–96.
[91] A. D. Becke, K. E. Edgecombe, *J. Chem. Phys.* **1990**, *92*, 5397–5403.
[92] R. F. W. Bader, *Atoms in Molecules: A Quantum Theory*, Oxford University Press, New York, USA, **1994**.
[93] D. Kozlowski, J. Pilmé, *Journal of Computational Chemistry* **2011**, *32*, 3207–3217.
[94] R. F. W. Bader, M. E. Stephens, *J. Am. Chem. Soc.* **1975**, *97*, 7391–7399.
[95] X. Fradera, M. A. Austen, R. F. W. Bader, *J. Phys. Chem. A* **1999**, *103*, 304–314.
[96] X. Fradera, J. Poater, S. Simon, M. Duran, M. Solà, *Theor. Chem. Acc.* **2002**, *108*, 214–224.

Entry for the Table of Contents

FULL PAPER

Halogen-bond strengths at variance with the evolution of substituent polarizability in astato-methanes.

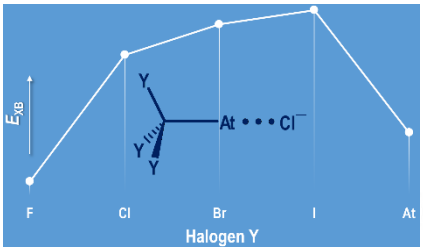

S. Sarr, J. Graton, G. Montavon, J. Pilmé, N. Galland**

Page No. – Page No.

On the interplay between charge-shift bonding and halogen bonding